Journal of Cerebral Blood Flow & Metabolism (2015) 35, 392–401

www.jcbfm.com

ORIGINAL ARTICLE

3D GRASE pulsed arterial spin labeling at multiple inflow times in patients with long arterial transit times: comparison with dynamic susceptibility-weighted contrast-enhanced MRI at 3 Tesla

Steve Z Martin[1,7], Vince I Madai[1,2,7], Federico C von Samson-Himmelstjerna[1,3], Matthias A Mutke[1,2], Miriam Bauer[1], Cornelius X Herzig[1], Stefan Hetzer[4], Matthias Günther[3,5,6] and Jan Sobesky[1,2]

Pulsed arterial spin labeling (PASL) at multiple inflow times (multi-TIs) is advantageous for the measurement of brain perfusion in patients with long arterial transit times (ATTs) as in steno-occlusive disease, because bolus-arrival-time can be measured and blood flow measurements can be corrected accordingly. Owing to its increased signal-to-noise ratio, a combination with a three-dimensional gradient and spin echo (GRASE) readout allows acquiring a sufficient number of multi-TIs within a clinically feasible acquisition time of 5 minutes. We compared this technique with the clinical standard dynamic susceptibility-weighted contrast-enhanced imaging–magnetic resonance imaging in patients with unilateral stenosis >70% of the internal carotid or middle cerebral artery (MCA) at 3 Tesla. We performed qualitative (assessment by three expert raters) and quantitative (region of interest (ROI)/volume of interest (VOI) based) comparisons. In 43 patients, multi-TI PASL-GRASE showed perfusion alterations with moderate accuracy in the qualitative analysis. Quantitatively, moderate correlation coefficients were found for the MCA territory (ROI based: $r = 0.52$, VOI based: $r = 0.48$). In the anterior cerebral artery (ACA) territory, a readout related right-sided susceptibility artifact impaired correlation (ROI based: $r = 0.29$, VOI based: $r = 0.34$). Arterial transit delay artifacts were found only in 12% of patients. In conclusion, multi-TI PASL-GRASE can correct for arterial transit delay in patients with long ATTs. These results are promising for the transfer of ASL to the clinical practice.

Journal of Cerebral Blood Flow & Metabolism (2015) **35,** 392–401; doi:10.1038/jcbfm.2014.200; published online 19 November 2014

Keywords: arterial spin labeling; ASL; cerebral blood flow; cerebrovascular disease; magnetic resonance; MRI; perfusion-weighted MRI

INTRODUCTION

Arterial spin labeling (ASL) is emerging as a noninvasive alternative magnetic resonance imaging (MRI) technique for the assessment of brain perfusion, where magnetically labeled blood serves as an endogenous contrast agent.[1,2] In the clinical setting, however, dynamic susceptibility-weighted contrast-enhanced imaging (DSC), applying Gadolinium-based exogenous contrast agents, is still the current standard.[3] In comparison with DSC, ASL offers some unique advantages. It is noninvasive, can be used for repetitive measurements, and is suitable for patients with contra-indications to Gadolinium-based contrast agents. To be of comparable clinical value, however, ASL should be readily available in the clinical setting (e.g., as a product sequence from a vendor) and should offer a diagnostic value equal to DSC in various neurologic diseases.[4–8] Among these, steno-occlusive disease is especially challenging for ASL because of increased arterial transit times (ATTs), which require long delays between labeling and image acquisition (usually >2 seconds) to ensure the arrival of labeled bolus in all voxels. As a consequence of T1 relaxation, the signal of labeled blood decays over time and decreases the signal-to-noise ratio (SNR), when a long imaging delay is used to account for long ATTs. To compensate for this, averaging over multiple repetitions of the measurement is necessary, but is not possible with all ASL sequences within clinically reasonable acquisition times. We confirmed this in a recent validation of an ASL product sequence in steno-occlusive disease, where we showed that brain perfusion could not be reliably assessed.[9] A very promising approach to solve this issue is the use of a three-dimensional (3D) gradient and spin echo (GRASE) readout module. It increases the SNR of a single measurement and allows scanning at multiple time points after labeling (inflow times = TIs) within approximately 5 minutes.[10] This

[1]Center for Stroke Research Berlin (CSB), Charité—Universitätsmedizin, Berlin, Germany; [2]Department of Neurology, Charité—Universtitätsmedizin, Berlin, Germany; [3]Fraunhofer MEVIS, Institute for Medical Image Computing, Bremen, Germany; [4]Berlin Center for Advanced Neuroimaging (BCAN), Berlin, Germany; [5]Faculty of Physics and Electronics, University of Bremen, Bremen, Germany and [6]mediri GmbH, Heidelberg, Germany. Correspondence: Professor Dr J Sobesky, Department of Neurology and Center for Stroke Research Berlin (CSB), Charité—Universitätsmedizin, Charitéplatz 1, Berlin 10117, Germany.
E-mail: jan.sobesky@charite.de
The research leading to these results has received funding from the German Federal Ministry of Education and Research via the grant 'Center for Stroke Research Berlin' (01EO 0801; http://www.bmbf.de). The funders had no role in study design, data collection and analysis, decision to publish, or preparation of the manuscript.
[7]These authors contributed equally to this work.
Received 26 June 2014; revised 26 September 2014; accepted 22 October 2014; published online 19 November 2014

approach yields bolus-arrival-time (BAT) maps in addition to cerebral blood flow (CBF) maps and subsequently corrects CBF for long ATTs, which is especially interesting for patients with steno-occlusive disease. Importantly, an implementation of this sequence has recently become commercially available for some scanner types[11] and the 3D GRASE readout is a recommended technique according to the latest international guidelines.[12] We therefore investigated the clinical performance of a 3D GRASE PASL sequence at multiple TIs (multi-TIs) in comparison with DSC-MRI in patients with atherosclerotic steno-occlusive disease.

MATERIALS AND METHODS

Ethics Statement

All patients gave informed written consent before the study. The study was conducted according to the principles expressed in the Declaration of Helsinki and was approved by the authorized institutional review board of the Charité—Universitätsmedizin Berlin.

Study Design

We performed an observational prospective imaging study (Perfusion imaging by ASL for clinical use in stroke—PEGASUS, WHO international Clinical trials registry no. DRKS00003198). Patients with steno-occlusive disease were recruited at the Department of Neurology of the Charité—Universitätsmedizin Berlin or presenting at our out-patient services between July 2012 and August 2014. Inclusion criteria were: (a) stenosis $>70\%$ of the internal carotid artery (ICA) or middle cerebral artery (MCA) according to the ECST (European Carotid Surgery Trial) criteria, (b) age 18 to 80 years, and (c) clinically and hemodynamically stable status. Grading of stenosis was confirmed before MRI by duplex sonography and/or computed tomography/MRI-angiography.

Exclusion criteria were: (a) magnetic implants, (b) claustrophobia, (c) aphasia or reduced level of consciousness, (d) severe allergic reactions in the previous medical history, (e) allergic reactions against Gadolinium-based contrast agents in the past, (f) renal insufficiency (defined by a glomerular filtration rate under ≤ 30 mL/min per 1.73 m^2, (g) pregnancy, (h) unstable clinical status, and (i) contralateral stenosis $>50\%$ (ECST criteria). For each patient, National Institute of Health Stroke Scale, Modified Rankin Scale and relevant clinical data were assessed before imaging.

Magnetic Resonance Imaging Hardware

Magnetic resonance imaging was performed on a 3 T whole-body system (Magnetom Trio, Siemens Healthcare, Erlangen, Germany) using a 12-channel receive RF coil (Siemens Healthcare, Erlangen, Germany) tailored for head imaging.

Magnetic Resonance Imaging Sequences

Arterial spin labeling imaging. We used a pulsed ASL (PASL) sequence with flow alternating inversion recovery (FAIR) labeling and a Q2TIPS[13,14] saturation scheme combined with a 3D GRASE readout[10] at multi-TIs. The ASL parameters were in detail: 15 TIs (start: 300 milliseconds, end: 3100 milliseconds, increment: 200 milliseconds), 3 averages per TI, bolus length = 1400 milliseconds, 1 frequency offset corrected inversion (FOCI) labeling pulse followed by 4 π/2-presaturation pulses and 2 FOCI background suppression pulses (optimized for suppression of T1 = 700 and 1400 milliseconds); 3D GRASE parameters were in detail: field of view = 256 × 160 mm, nominal voxel size = 4.0 × 4.0 × 4.0 mm^3 (interpolated to 2.0 × 2.0 × 4.0 mm^3), 26 slices, repetition time (TR)/echo time (TE) = 3620 /24.78 milliseconds, flip angle (refocusing pulses) = 100°, number of segments = 1 (single-shot), time of acquisition = 5:26 minutes, turbo factor = 16, echo planar imaging (EPI)-factor = 48, partial fourier (with zero filling in z direction) = 5/8, Bandwidth = 2298 Hz/Pixel.

Dynamic susceptibility-weighted contrast-enhanced imaging. The DSC-MRI protocol consisted of a series of 80 whole-brain images using a single-shot free induction decay (FID)-EPI sequence. DSC parameters were in detail: field of view = 224 × 224 mm, voxel size = 1.8 × 1.8 × 5 mm^3; slices = 21; acceleration factor = 2; TR/TE = 1390 /29 milliseconds; flip angle = 60°; time of acquisition = 1:54 minutes; 5 mL Gadovist (Gadobutrol, 1 mol/L; Bayer Schering Pharma AG, Berlin, Germany) followed by a 25 mL saline flush were injected using a power injector (Spectris, Medrad, Warrendale PA, USA) at a rate of 5 mL/seconds. DSC-MRI was performed immediately after ASL imaging.

Magnetization prepared rapid gradient-echo imaging. As an anatomic reference, we used a 3D, T1-weighted, magnetization prepared rapid gradient-echo (MPRAGE) sequence with the following parameters: voxel size = 1.0 × 1.0 × 1.0 mm^3; TR/TE = 1900/2.25 milliseconds; time of acquisition = 4:26 minutes.

Data Postprocessing

Arterial spin labeling imaging. The ASL time series data were postprocessed with an in-house software package based on MeVisLab 2.5 (MeVis Medical Solutions, Bremen, Germany). First, the MPRAGE image was reformatted to the transversal orientation and then to the ASL time series to improve the power of skull stripping. Next, the original ASL perfusion map was coregistered with the skull stripped MPRAGE image. The computed transformation matrix was used on the ASL parameter maps. In addition, a presubtraction Gaussian smoothing of 2 mm was applied to avoid subtraction errors. For the quantitative analysis DSC-CBF and DSC-time-to-peak (TTP) maps were also coregistered with the skull stripped MPRAGE image. For coregistration, a rigid transformation and linear registration was used.

In the following step, ASL perfusion data were fitted to a model function by using an implementation of the Levenberg-Marquardt algorithm (mpfit, http://www.physics.wisc.edu/~craigm/idl/cmpfit.html). As the model function, the General Kinetic Model by Buxton *et al*[15] was used. The following parameter assumptions were made: $\lambda = 1$, T1 of arterial blood = 1600 milliseconds, T1 of brain tissue = 1200 milliseconds, and bolus length = 1400 milliseconds. The following maps were created: (a) ASL-CBF and (b) ASL-BAT.

Dynamic susceptibility-weighted contrast-enhanced imaging. Dynamic susceptibility-weighted contrast-enhanced imaging-MRI images were postprocessed offline with Perfusion Mismatch Analyzer (version 3.4.0.6, ASIST Japan, Iwate, Japan) generating TTP (DSC-TTP) maps. In addition, for the quantification of CBF (DSC-CBF), four arterial input functions were placed manually in the M1 branch contralateral to the affected hemisphere[16] and CBF was calculated using block circulant singular value decomposition deconvolution (bSVD) with an oscillation index algorithm (oscillation index: 0.095). A fixed threshold level of 0.2 was used as the cutoff value for diagonal matrices. This technique was found to be insensitive to prolonged ATTs.[17,18]

Qualitative Analysis

Maps of ASL-CBF, ASL-BAT, DSC-CBF, and DSC-TTP were visually assessed by three readers masked to clinical data (JS, 11 years of experience in stroke perfusion imaging; VIM, 5 years; SZM, 3 years; all readers have specific expertise in ASL imaging). Results were obtained by majority rating. The rating was performed after a predefined standardized algorithm: ASL and DSC maps were rated in separate reading sessions. Imaging quality was rated as 'very good' (1), 'good' (2), 'sufficient' (3), or 'uninterpretable' (4). Image quality between modalities was then compared using the Wilcoxon signed rank test. Raters were asked to rate for type (CBF: hyperperfusion, hypoperfusion, normal perfusion; BAT and TTP: increase, unchanged) and location (anterior cerebral artery (ACA); MCA; posterior cerebral artery (PCA)) of perfusion abnormality and to note any side difference. Sensitivity and specificity of ASL-CBF maps to predict hypoperfusion and of ASL-BAT maps to predict TTP delay was calculated. Reference for normal ASL-BAT maps was MacIntosh *et al*.[19] In addition, raters were asked to note the appearance of artifacts owing to increased ATTs, the 'arterial transit delay artifact' (ATDA) in ASL-CBF maps.[9] Using the additional information provided by BAT maps, ATDAs were defined by the occurrence of hyperintense dots in an area of low signal intensity in ASL-CBF with a corresponding increase of ASL-BAT in this area. Interrater agreement was assessed using Randolph's free-marginal multirater kappa.[20,21]

Quantitative Analysis

The coregistered maps of MPRAGE, ASL-CBF, ASL-BAT, DSC-CBF, and DSC-TTP were resliced to DSC map voxel dimensions using Vinci 4.18 (Max-Planck-Institute for Neurological Research, Cologne, Germany).[22]

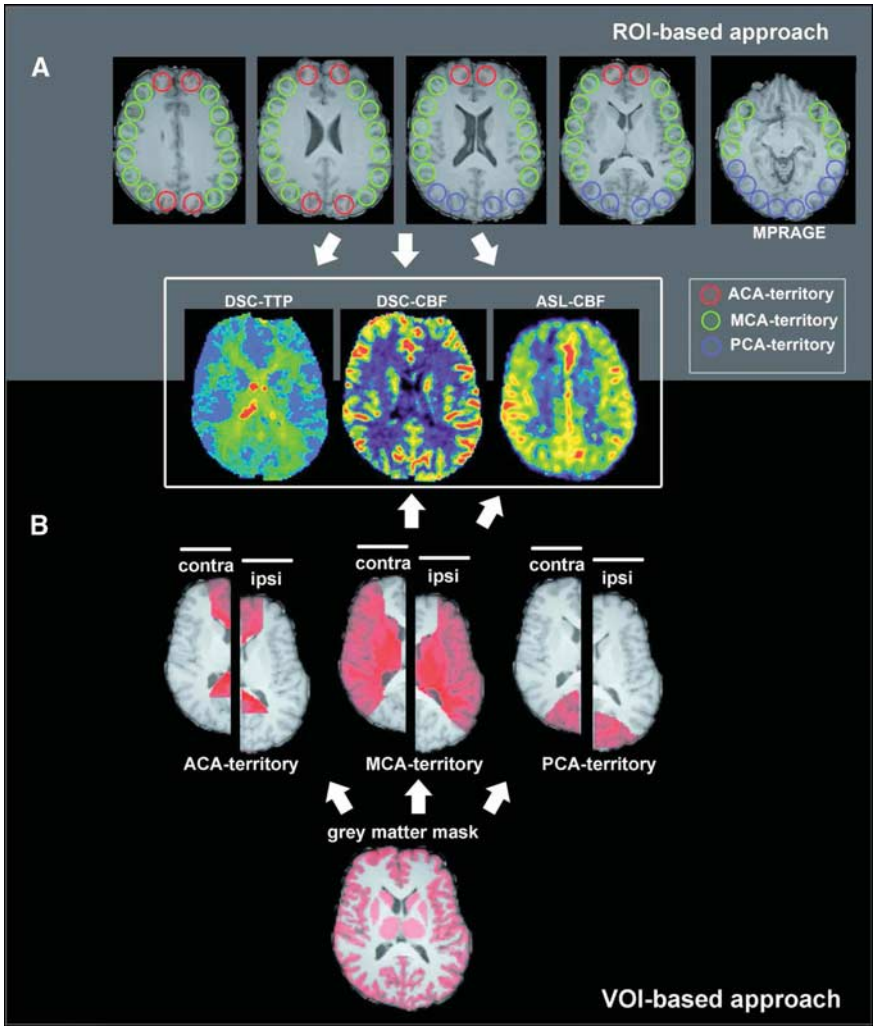

Figure 1. Quantitative analysis of dynamic susceptibility-weighted contrast-enhanced imaging (DSC) and arterial spin labeling (ASL) images. (**A**) In all, 20 mm circular regions of interest (ROIs) were placed on the magnetization prepared rapid gradient-echo (MPRAGE) image and copied onto coregistered DSC-time-to-peak (TTP), DSC-cerebral blood flow (CBF), and ASL-CBF images. ROIs are colored according to the vascular territory. For relative values, the ratio of each ipsilateral ROI was divided by the mean of all contralateral ROIs of the same vascular territory. In case of DSC-TTP, the values were subtracted from the mean TTP value of all contralateral ROIs. (**B**) Gray matter masks, perfusion territory masks for anterior cerebral artery (ACA), middle cerebral artery (MCA), and posterior cerebral artery (PCA) were both placed onto DSC-CBF and ASL-CBF images and relative mean values were obtained (mean value of the ipsilateral perfusion territory divided by the mean value of the respective contralateral perfusion territory).

Volume of interest (VOI)-based analysis. Gray matter masks based on MPRAGE data were created offline using MIPAV (Medical Image Processing, Analysis and Visualization, version 7.0.1, Bethesda, MD, USA) and MeVisLab. First, skull stripping (brain surface extraction (BSE) module) and automatic gray matter segmentation (single channel fuzzy c-means) were performed using MIPAV. All following steps were performed using MeVisLab: gray matter masks were manually corrected for misclassified voxels. Hemisphere masks (both ipsilateral and contralateral) and perfusion territory masks for ACA, PCA, and MCA territories were manually created, the latter on the basis of established flow territory templates.[23] CBF mean values were obtained placing both masks (gray matter and perfusion territory mask) onto ASL-CBF and DSC-CBF maps. Relative CBF (relCBF) values were calculated dividing the mean value of the ipsilateral perfusion territory by the mean value of the respective contralateral perfusion territory (%) (for a schematic overview of our methodology, see Figure 1).

Region of interest (ROI)-based analysis. Per slice and hemisphere 7 to 8 (dependent on brain size) cortical circular ROIs (diameter: 20 mm) were placed on five axial slices. Slices above the lateral ventricles and slices incorporating the cerebellum were not included. ROIs were placed on MPRAGE images and copied on ASL-, DSC-CBF, and DSC-TTP maps (see Figure 1). ROIs were labeled according to the vascular territory they were placed in and their position relative to the side of steno-occlusion (ipsilateral or contralateral). RelCBF values were calculated by dividing the mean value of each ipsilateral ROI value by the mean of all contralateral ROIs of the same vascular territory. Relative TTP values for ipsilateral ROIs were obtained by subtraction of the mean TTP value of all contralateral ROIs.

In a second quantitative ROI and VOI analysis, regions with ATDA were excluded. As ATDAs were found exclusively in the MCA perfusion territory, this step was only performed for the MCA regions (VOI based: all MCA-VOI values of patients showing ATDA were excluded from the analysis; ROI based: all MCA-ROI values of patients showing ATDA were excluded from the analysis). In addition, to analyze the impact of very long transit times, ROIs were classified as within (group 1) or beyond (group 2) our maximum TI (3.1 seconds) based on TTP. Then, the ratio ASL-relCBF/DSC-relCBF was calculated using each pair of corresponding ROIs. The ratios of the groups 1 and 2 were compared using the Mann–Whitney *U* rank sum test.

Table 1. Clinical data of all patients

Patient number	*Sex*	*Age (y)*	*NIHSS (p)*	*Stroke*	*TIA*	*GoS (%) ICA right*	*GoS (%) ICA left*	*GoS (%) MCA right*	*GoS (%) MCA left*
1	M	76	0	x		>70%			
2	M	31	0	x			100%		
3	M	78	0		x	40–50%	70%		
4	W	63	0	x		40%	40%	>70%	50%
5	W	37	0				100%		
6	W	49	0	x			100%		
7	W	73	0			70%	30%		
8	M	48	0				70–80%		
9	M	46	0	x			100%		
10	W	73	0		x		>70%		
11	M	60	0		x		70–80%		
12	M	65	0				100%		
13	W	74	0			80%			
14	M	58	0		x		86–99%		
15	M	68	0	x		70–80%			
16	W	49	0	x		100%			
17	W	72	0	x					>80%
18	M	47	2	x		100%			
19	M	51	3	x			40%	100%	
20	M	51	3	x		100%			
21	M	39	7	x			100%		
22	M	49	0				>70%		
23	W	41	0			50%	100%		
24	M	62	2	x		100%			
25	M	54	8	x		80%			
26	M	57	2	x		30–40%	30–40%	100%	
27	M	62	10	x		100%	50%		
28	M	57	1	x			100%		
29	M	30	0		x			>70%	
30	M	82	0	x			70–80%		
31	M	65	7	x		50%	100%		
32	M	57	0		x		100%		
33	M	68	0	x			100%		
34	W	42	1	x		50%	>70%		
35	W	74	0	x		30%	70%		
36	M	64	0	x			100%		
37	M	70	0	x		70%	50%		
38	M	69	0			90%	30%		
39	M	53	0		x		100%		
40	M	74	0			80–90%	40%		
41	M	78	0	x		80–90%			
42	W	75	0				80%		
43	M	66	0			50%	70%		

GoS, grade of stenosis; NIHSS, National Institute of Health Stroke Scale; ICA, internal carotid artery; M, man; MCA, middle cerebral artery; p, points; W, woman; y, years.

Statistical Analysis

Normalized VOI and ROI values of ASL-CBF were plotted against DSC-CBF and compared using Spearman's correlation coefficient. In addition, the Bland–Altman plot was used for comparison. For statistical analysis, we used sigmaplot 11.0 (Systat Software, San Jose, CA, USA) and for Bland–Altman plots, we used MedCalc 12.7.5.0 (MedCalc Software bvba, Ostend, Belgium).

Correction of Susceptibility Artifact

In our qualitative analysis, we identified a readout related frontal sinus susceptibility artifact owing to the right–left phase encoding direction. For three patients, additionally performed ASL measurements in the left–right phase encoding direction were available. This made it possible to correct susceptibility artifacts using the TOPUP tool implemented in FMRIB Software Library (FSL).[24,25] Here, from a pair of images (tag image, TI = 1300 ms) with right–left and left–right phase encode directions, a susceptibility-induced off-resonance field was estimated, which was then applied to all ASL images (for one exemplary patient, see Figure 4).

RESULTS

Forty-three patients met the inclusion criteria and completed the imaging protocol. Median age of all patients was 59 years, 25 patients had previous stroke, 7 patients had previous transient ischemic attack. Twelve patients were female. Detailed clinical data are shown in Table 1.

In the quality rating, none of the DSC and ASL maps were rated uninterpretable. DSC maps were found to show significantly better image quality than ASL maps (mean ASL-CBF: 2.0 versus mean DSC-CBF: 1.8, $P = 0.003$; mean ASL-BAT 3.0 versus mean DSC-TTP: 2.1, $P < 0.001$).

In the qualitative analysis, ASL-CBF showed in the MCA and PCA territory moderate-to-high sensitivity for the detection of DSC hypoperfusion (MCA 82%; PCA 75%) and moderate specificities (MCA 67%; PCA 66%). In the ACA perfusion territory, a consistently right-side hypointensity was found in the majority of ASL images (90%), which deteriorated the prediction of DSC hypoperfusion

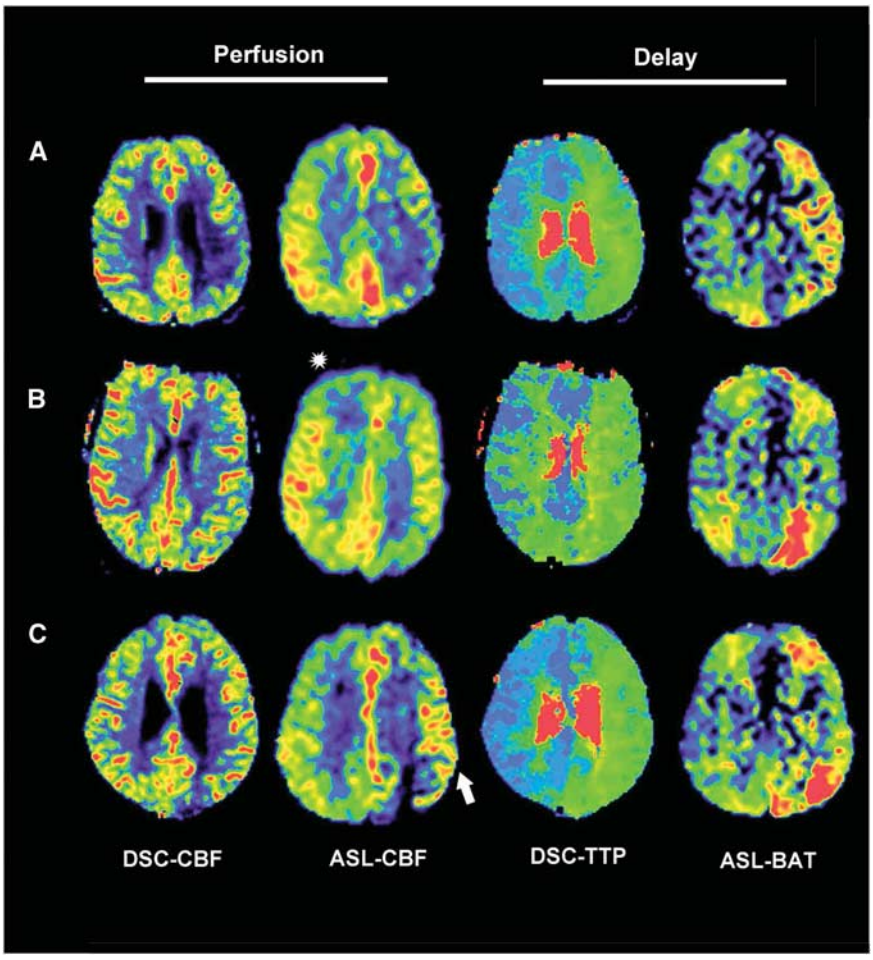

Figure 2. Exemplary patients. (**A**) A 39-year-old male, occlusion of the left internal carotid artery (ICA). Dynamic susceptibility-weighted contrast-enhanced imaging (DSC)-cerebral blood flow (CBF) shows a hypoperfusion in the lower part of the left middle cerebral artery (MCA) vascular territory. The arterial spin labeling (ASL) perfusion image shows matching perfusion changes as DSC-CBF. Time-to-peak (TTP)-DSC shows an ipsilateral delay (relative TTP (relTTP) = 3 seconds) of the whole left MCA territory. This ipsilateral delay is also visible in the ASL-bolus-arrival-time (BAT) map. (**B**) A 48-year-old male, 99% stenosis of the left ICA. DSC-CBF shows a slight hypoperfusion in the left MCA vascular territory. ASL-CBF confirms this finding in the same area, but additionally shows an area of stronger CBF hypoperfusion in the posterior cerebral artery (PCA) territory. Note corresponding increased intensity in the BAT map and also the right frontal hypointense artifact in ASL-CBF (asterisk) (**C**) A 57-year-old male, occlusion of the left ICA. DSC-CBF shows a slight hypoperfusion in the left MCA vascular territory. ASL-CBF confirms this finding. However, ASL-CBF shows also arterial transit delay artifacts in this area evidenced by hyperintense serpiginous and dot shaped signals (white arrow). Both, TTP-DSC and ASL-BAT show a corresponding ipsilateral delay (relTTP = 2.8 seconds).

(ACA sensitivity/specificity: 50%/54%; see Figure 4). ASL-BAT, however, showed moderate-to-high sensitivity for the detection of TTP delay (ACA 83%, MCA 67%) and moderate specificity (ACA 68%, MCA 71%) in the ACA and MCA territory. In the PCA perfusion territory, ASL-BAT maps showed only a weak-to-moderate sensitivity/specificity (50%/76%) and a moderate inter-rater agreement with a kappa of 0.66. There was a high interrater agreement with a kappa of >0.73 for all other maps. In 5 of 43 patients (12%), ATDA was identified in the MCA territories in ASL-CBF; ACA and PCA territories showed no such artifacts (for exemplary patient, see Figure 2C). Details of the qualitative analysis can be found in Tables 2 and 3 and online in the supplement (Figures 2 and 3). Exemplary results of the visual analysis are shown in Figure 2. In the quantitative analysis, we found a significant moderate correlation for DSC-relCBF versus ASL-relCBF in the MCA territory (ROI based: $r = 0.52$; volumetric based: $r = 0.48$) and significant weak correlations for the ACA and PCA territory (ROI based: $r = 0.29$ versus 0.42; volumetric based: $r = 0.34$ versus 0.32). After exclusion of ATDA, the correlation coefficients for ROI-based analysis were unchanged, whereas in the VOI-based analysis the correlation coefficient for the MCA territory increased to a correlation of $r = 0.62$. See Figures 3A and 3B for plots of the quantitative analysis.

In total, 1,605 pairs of ASL-CBF versus DSC-CBF ROIs were applied in the patient cohort. Of these, 1,485 (92%) showed a TTP delay, which was within our longest TI of 3.1 seconds. Only 120 (8%) showed a TTP delay of >3.1 seconds. The ratio ASL-CBF/DSC-CBF was significantly lower in the group with TTP delay of >3.1 seconds. This indicates underestimation of CBF by ASL, when TTP is >3.1 seconds (for details, see Figure 3C).

DISCUSSION

We report on the performance of a multi-TI pulsed ASL sequence with 3D GRASE readout to assess perfusion in patients with steno-occlusive disease of the brain in comparison with the clinical standard DSC-MRI. ASL maps identified changes in DSC imaging with moderate precision. In addition, we found a moderate significant correlation of ASL-CBF values with DSC-CBF values. In the ACA territory, we described a frequently occurring right-sided

Table 2. Qualitative visual rating: DSC-CBF versus ASL-CBF

		DSC-CBF					
		ACA territory		MCA territory		PCA territory	
		Hypoperfusion	No hypoperfusion	Hypoperfusion	No hypoperfusion	Hypoperfusion	No hypoperfusion
ASL-CBF	Hypoperfusion	3	17	23	5	6	12
	No hypoperfusion	3	20	5	10	2	23
		Sens./Spec.: 50%/54%		Sens./Spec.: 82%/67%		Sens./Spec.: 75%/66%	

ACA, anterior cerebral artery; ASL, arterial spin labeling; CBF, cerebral blood flow; DSC, dynamic susceptibility-weighted contrast-enhanced imaging; MCA, middle cerebral artery; MRI, magnetic resonance imaging; PCA, posterior cerebral artery; Sens., sensitivity; Spec., specificity. Results of the visual qualitative analysis**:** all data relate to the hemisphere ipsilateral to the steno-occlusion. Table shows visual findings for ASL-CBF versus DSC-CBF. Rows show imaging findings for ASL, columns show imaging findings for DSC. Sens. and Spec. indicate the ability of ASL to predict imaging findings of DSC-MRI.

Table 3. Qualitative visual rating: DSC-TTP versus ASL-BAT

		DSC-TTP					
		ACA territory		MCA territory		PCA territory	
		Delay	No delay	Delay	No delay	Delay	No delay
ASL-BAT	Delay	5	12	24	2	11	5
	No delay	1	25	12	5	11	16
		Sens./Spec.: 83%/68%		Sens./Spec.: 67%/71%		Sens./Spec.: 50%/76%	

ACA, anterior cerebral artery; ASL, arterial spin labeling; BAT, bolus-arrival-time; DSC, dynamic susceptibility-weighted contrast-enhanced imaging; MCA, middle cerebral artery; MRI, magnetic resonance imaging; PCA, posterior cerebral artery; Sens., sensitivity; Spec., specificity; TTP, time-to-peak. Results of the visual qualitative analysis**:** all data relate to the hemisphere ipsilateral to the steno-occlusion. Table shows visual findings for ASL-BAT versus DSC-TTP. Rows show imaging findings for ASL, columns show imaging findings for DSC. Sens. and Spec. indicate the ability of ASL to predict imaging findings of DSC-MRI.

artifact, which impaired identification of changes in DSC hypoperfusion.

Arterial spin labeling is an evolving technique for the assessment of brain perfusion[2,26] and its use in the clinical setting is encouraged.[2,12,27] One very promising technique is a state-of-the-art pulsed ASL labeling sequence with 3D GRASE readout applying measurements at multi-TIs, which holds the potential to correct for long ATTs.[10] Latest international guidelines[12] recommended ASL settings for clinical use, however, these were exclusively aimed at single-TI ASL techniques. No recommendations exist for multi-TI techniques, although its use is encouraged for patients suffering from steno-occlusive disease. In this respect, we aimed to validate 3D GRASE PASL at multi-TIs in direct comparison with the clinical standard DSC-MRI. Both sequences were used within one session in patients with unilateral hemodynamically relevant steno-occlusive disease of the brain and at a field strength of 3 Tesla.

Three reasons make the analyzed 3D GRASE ASL sequence especially suited to be used in patients with long arterial delay times. First, it offers very high SNR[10] per single image acquisition. This allows obtaining sufficient SNR also at very long TIs applying three averaging steps in only 21 seconds. Therefore, we are able to acquire multi-TIs within a clinically relevant acquisition time of 5:26 minutes. Second, the acquisition of information at multi-TIs allows for the measurement of the arrival of the bolus within regional tissue. This information makes it possible to calculate BAT maps and to correct CBF maps giving accurate information about CBF also in regions with very long transit times. Third, as an image of a 3D volume can be acquired in one single-shot, perfusion can be measured in the whole brain at the same time. This is in contrast to other readout techniques like 2D EPI, where perfusion has to be measured slice per slice and where each slice corresponds to a different acquisition time.

Applying a 3D GRASE ASL sequence in this study in a cohort of patients with unilateral hemodynamically relevant chronic stenosis of the anterior circulation, we found that BAT maps had moderate accuracy to identify areas of prolonged transit delay in the ACA and MCA perfusion territory and we found a significant moderate correlation of BAT-corrected ASL-CBF to DSC-CBF. Also, ATDAs were found with 12% in a very low number of patients in contrast to 76% in the study of Mutke *et al*,[9] who investigated a comparable study population with a PASL sequence at a single-TI of 1.7 seconds. This is supported by our quantitative finding that only 8% of ROIs showed a relative TTP delay above 3.1 seconds, the longest TI we used. It should be noted, however, that the direct comparison of relative TTP delay with the ASL TI is an approximation and is not validated. Our results are in line with a unimodal pilot study applying a 3D GRASE PASL sequence in a heterogeneous cohort of patients with minor stroke, where the authors concluded that BAT maps can be used to identify perfusion abnormalities as a result of long transit times.[28] Furthermore, in the study of Mutke *et al*,[9] 39% of the ASL images were rated uninterpretable because of severe patient motion artifacts and had to be excluded from analysis. Using the 3D GRASE ASL sequence in our study, no ASL image was rated uninterpretable and all images could be analyzed. This suggests that the used single-shot 3D GRASE readout is less prone to motion artifacts and is therefore suited for a patient sample reflecting clinical conditions.

Only two previous reports compared ASL with DSC-MRI in patients with chronic steno-occlusive disease. In the mentioned study of Mutke *et al*[9] applying a single-TI PASL sequence with 2D EPI readout, it was shown that transit delay artifacts in these patients were so prominent that assessment of ASL-CBF was not possible with a very weak correlation between ASL-CBF and DSC-CBF. Yun *et al*[29] applied a single time point pseudocontinuous

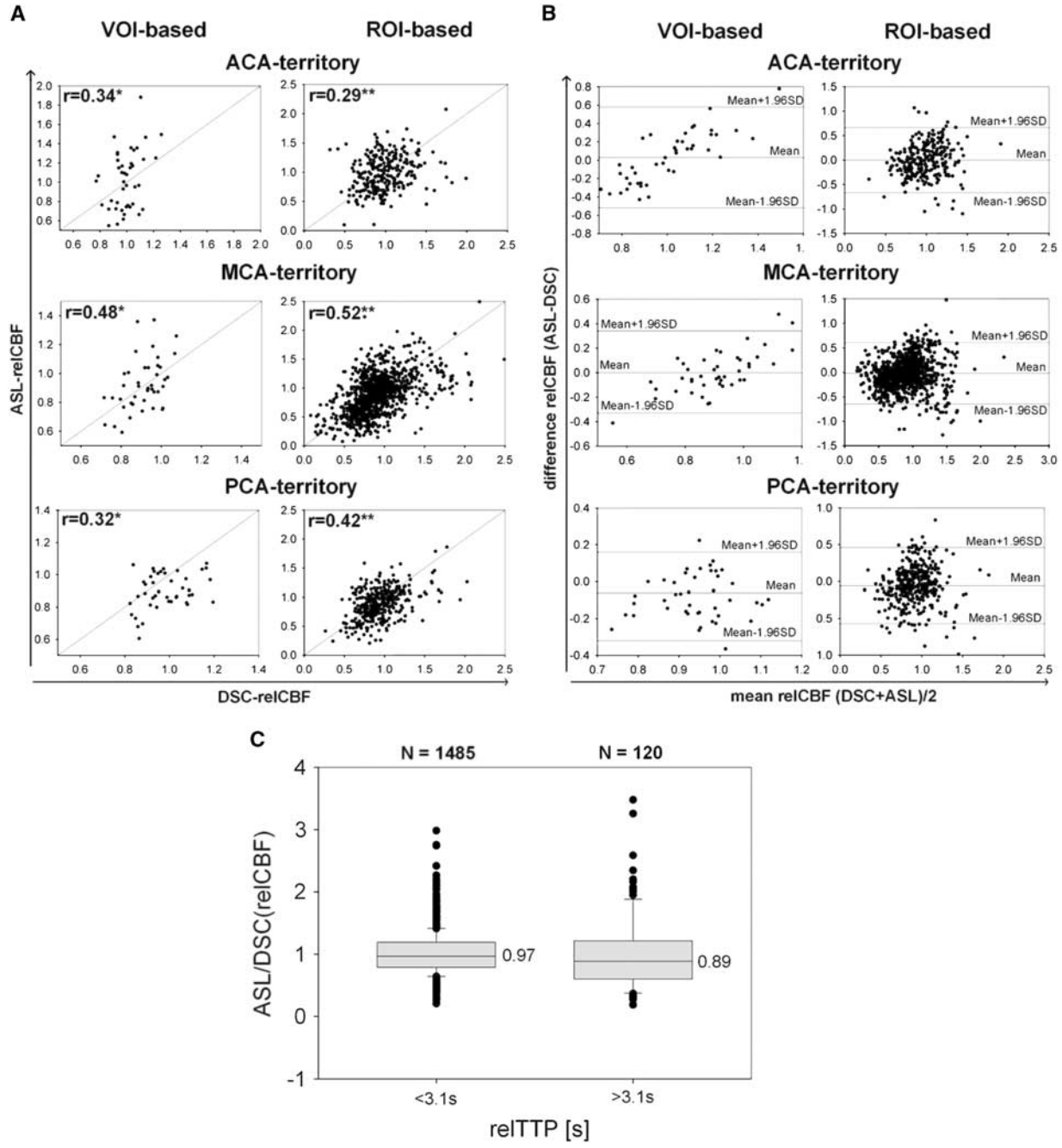

Figure 3. Scatter plots and Bland-Altman (BA) plots. Data of all 43 patients are shown. (**A**) Scatter plots comparing dynamic susceptibility-weighted contrast-enhanced imaging (DSC)-relative cerebral blood flow (relCBF) and arterial spin labeling (ASL)-relCBF of the volume-of-interest (VOI)-based and the region of interest (ROI)-based analysis are depicted for each vascular territory ipsilateral to the steno-occlusion. The respective correlation is shown (*$P < 0.05$; **$P < 0.0002$). (**B**) BA plots for all vascular- perfusion territories and for VOI- and ROI-based analysis are shown comparing DSC-relCBF and ASL-relCBF. BA plots for anterior cerebral artery (ACA) and middle cerebral artery (MCA) perfusion territory show a mean difference between DSC-relCBF and ASL-relCBF measurements of close to 0 (ACA (VOI, ROI) = (0.03, 0)/MCA (VOI, ROI) = (0, −0.02)) and for posterior cerebral artery (PCA) perfusion territory of −0.07 (PCA (VOI, ROI) = (−0.08, −0.06)). In the VOI-based approach, a spread of ±30% (MCA/PCA) and ±55% (ACA) and in the ROI-based approach of ±60% is seen within ±1.96 s.d. BA plots of the VOI-based analysis for the ACA and MCA territory show high differences for high average relCBF. This might be explained by overestimation of CBF because of macrovascular signals. In the ACA territory, there is an additional bias of the BA plot, probably because of the susceptibility artifacts. (**C**) All ROIs of the ipsilateral hemisphere were grouped according to a relative TTP (relTTP) delay of >3.1 seconds and <3.1 seconds (3.1 seconds being the highest TI used for ASL in our study). Only 8% ($n = 120$) ROI values were above 3.1 seconds. The ratio (relCBF-ASL/relCBF-DSC) was calculated for both groups and compared. The median of this quotient was significantly lower for ROIs with a relTTP delay of >3.1 seconds (0.97 versus 0.89, $P < 0.001$).

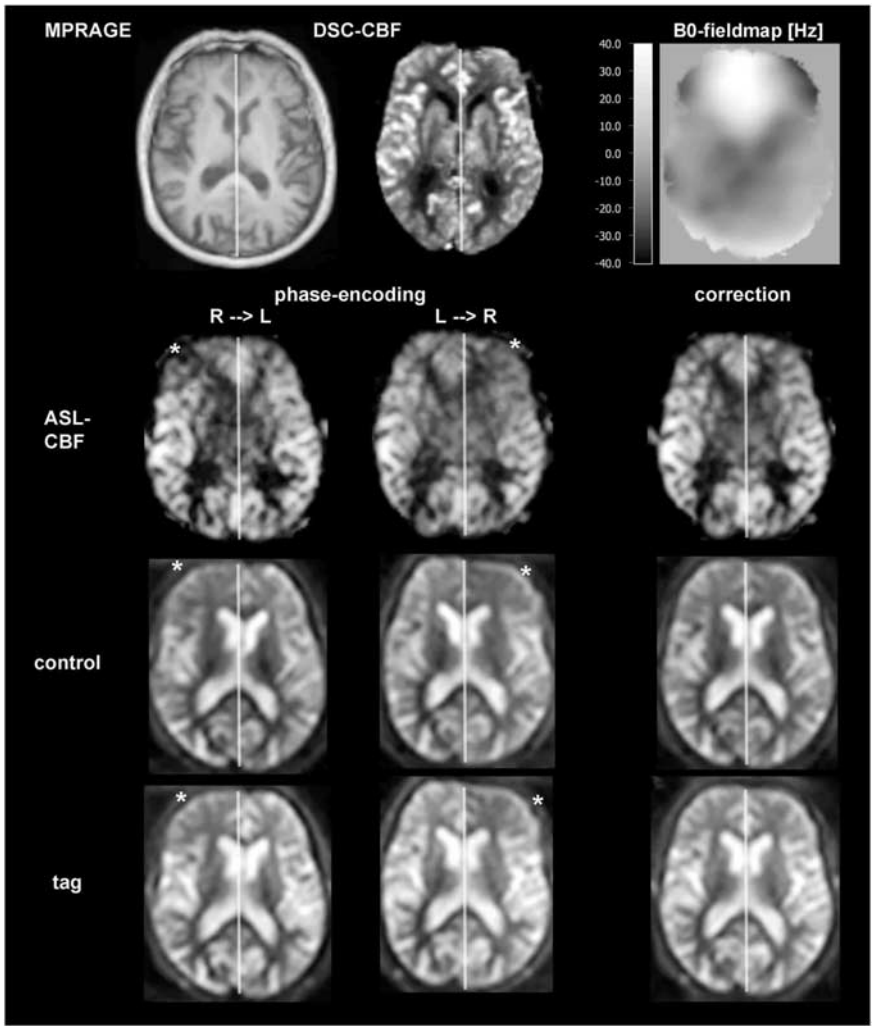

Figure 4. Example of the frontal sinus susceptibility artifact. A 78-year-old male, 80% to 90% stenosis of right internal carotid artery (ICA). Arterial spin labeling (ASL)-cerebral blood flow (CBF) image shows a hypointensity (asterisk) in the anterior cerebral artery (ACA) territory, which is not confirmed by dynamic susceptibility-weighted contrast-enhanced imaging (DSC)-CBF. This hypointensity is located on the right side for right–left (R–L) phase encoding direction and on the left side for left–right (L–R) phase encoding direction. It is visible in tag and control images (inflow time (TI) = 1300 milliseconds). In addition, considerable left to right (R–L) and right to left (L–R phase encoding direction) distortion is visible in the ASL-CBF, tag, and control images. The source is a frontal sinus susceptibility artifact. We have run a correction of this susceptibility artifact using TOPUP implemented in FMRIB Software Library (FSL), which successfully corrects for the distortions and the frontal artifact in ASL-CBF, tag, and control images. In addition, a B0-fieldmap is shown that has been scaled from − 40 Hz (corresponds black) to +40 Hz (corresponds white). Both geometrical and intensity distortions are corrected as indicated by the hyperintense field above the roof of the sinuses.

ASL (pCASL) sequence with a short postlabeling delay (PLD) of 1.5 seconds and a 3D spiral fast spin-echo (FSE) readout in patients with Moya-Moya disease using a 1.5 T system. Surprisingly, very high correlations of ASL-CBF and DSC-CBF up to $r = 0.90$ were found. Given that Moya-Moya patients display irregular collaterals and very high delay times, the high correlation in the study of Yun *et al* is challenging to explain, especially as correlations of ASL-CBF with a gold standard (Xenon-CT) in a similar collective led to much lower correlation values.[30,31] Taken together, the moderate correlation of up to $r = 0.52$ using 3D GRASE PASL in our study shows a clear improvement compared with the single-TI PASL sequence applied by Mutke *et al.*[9]

Alternative state-of-the-art labeling and readout techniques can be applied in patients with long arterial transit delay times. A look-locker approach PASL technique (QUASAR), which allows for multi-delay measurements was validated with 15O-water positron emission tomography with correlations of $r = 0.63$ (ref. 32) and $r = 0.69$ (ref. 33) between ASL-CBF and positron emission tomography-CBF and a correlation of 0.92 (ref. 34) in comparison with SPECT imaging. It can be expected that QUASAR leads to similar results as multi-TI 3D GRASE PASL when compared with DSC-MRI. However, as QUASAR applies a 2D EPI readout, longer scanning times might be necessary, when long delay times like 3.1 seconds as in our study have to be measured with comparable SNR. Next to PASL, labeling using pCASL is a promising approach because of higher achievable SNR. pCASL at multiple PLDs with a 3D spiral FSE readout was validated against Xenon-CT in a recent publication. Here, Qiu *et al*[30] measured the longest delay after labeling to date (4.5 seconds) and found a correlation of $r = 0.65$ in patients with Moya-Moya disease. However, to achieve adequate SNR at long PLDs, scanning times exceeded clinically feasible limits. Although this 3D pCASL approach is promising, the combination of multi-PLD pCASL labeling with a 3D GRASE readout could achieve comparable SNR at shorter scanning times.

Such an approach already led to very high correlations in comparison with perfusion computed tomography for 17 Moya-Moya patients in a recent study.[35] Thus, a multi-time point pCASL labeling with 3D GRASE readout approach should be evaluated in future studies in comparison with DSC-MRI in patients with steno-occlusive disease.

Although our results were promising for the MCA perfusion territory, the presence of a right-sided hypointense artifact severely limited the performance of ASL in the ACA territory. We identified a readout related frontal sinus susceptibility artifact as the cause, which becomes prominent in the right ACA territory owing to the right–left phase encoding direction (see Figure 4). Although Wang *et al*[35] did not report an artifact in their study using a multi-PLD pCASL GRASE in comparison with perfusion computed tomography, it might explain the very weak correlation in the ACA territory ($r = 0.26$) in contrast to very high correlation in the MCA territory ($r = 0.90$). Right to left phase encoding direction using 3D GRASE is beneficial, because the shape of the human head makes it possible to apply a rectangular field of view. This allows reducing the number of phase encoding steps, which leads to a shorter echo train and, thus, better image quality. As the presence of this artifact is readout specific and the 3D GRASE readout is a recommended technique according to the latest guidelines,[12] a solution for the artifact is highly warranted. On one hand, the acquisition of multiple segments could reduce the presence of the artifact. However, to achieve clinically feasible acquisition times, the number of averages per TI and/or the number of TIs would have to be decreased. However, an elegant technique for the correction of susceptibility artifacts in MR scans is available (http://www.diffusiontools.com/[36]; http://fsl.fmrib.ox.ac.uk/fsl/fslwiki/TOPUP[24,25]). This technique requires the acquisition of two images using the same readout, but with opposing phase encoding directions. We suggest that this correction should be implemented in 3D GRASE postprocessing routines (for an exemplary correction, see Figure 4).

From a clinical point of view, ASL implementations are needed that can be applied as an 'out-of-the-box' solution in the clinical setting. Prescan adaptation of ASL parameters to known transit delays might be appropriate for scientific validation studies and for follow-up examinations, but is not the primary goal of clinical imaging, where a fast screening tool is needed. To optimize sequences for clinical use, it is therefore necessary to find the best compromise between acquisition time, SNR, image resolution, and depiction of transit delay.[37] Unfortunately, the majority of studies with ASL were performed either in healthy volunteers or in patients without transit delay and these results were the basis of current guidelines, which predominantly address the use of single time point ASL.[12] If patients with transit delays were included, often Moya-Moya disease was investigated.[29–31,35,38] Moya-Moya disease, however, leads to extreme transit delays and is rare. Atherosclerotic steno-occlusive disease, in contrast, is frequent and shows moderate transit delay. Only a few studies compared ASL with other imaging techniques in chronic atherosclerotic steno-occlusive disease[9,32–34] (for an overview, see online Supplementary Figure 1). There is a need to validate ASL solutions, preferably multi-time and product sequences, in steno-occlusive disease to specify ASL parameters according to clinical requirements. In this respect, our findings suggest that a 3D GRASE readout meets the requirements of an out-of-the-box solution. Given its inherently high SNR, multiple averaging at long TIs as well as clinically feasible acquisitions times can be achieved as shown in our study. Moreover, BAT maps were an indicator of perfusion delay and yielded valuable additional information for cerebrovascular imaging.

Our study has several limitations. First, perfusion changes between measurements cannot be ruled out completely owing to the heterogeneity of perfusion status in patients with steno-occlusive disease. However, DSC-MRI followed ASL immediately and no change of clinical status between scans has been observed. Second, DSC and ASL display different pathophysiological pathways. ASL uses blood as a freely diffusible tracer, whereas Gadolinium stays intravascular, especially in the chronic state with an intact brain–blood barrier. In addition, the time resolutions of the methods are different. Applying a multi-TI approach, changes as small as 200 milliseconds can be measured with ASL, while the time resolution of DSC-MRI is limited by the TR (1.39 seconds in our study). Third, we used block circulant singular value decomposition deconvolution for the postprocessing of DSC-MRI images. Although this deconvolution method is thought to be much more delay insensitive than standard deconvolution methods (standard singular value decomposition (sSVD)),[17,18] this advantage has been only shown in small pilot studies and sSVD deconvolution is more widely used in the clinical setting. Fourth, a verification of the bolus length of 1400 milliseconds in the fitting routine might improve ASL maps and should be considered in future multi-TI studies. Fifth, small ROIs used in our quantitative analysis have high sensitivity for regional changes, but are prone to spatial errors. Given, however, that the results of a large VOI analysis showed comparable results, it is likely that spatial errors had only limited effect on our analysis. Sixth, we have not assessed whether signal decay because of T2 had an effect on the effective resolution of our ASL sequence. It is possible to simulate point spread functions for this purpose (see Vidorreta *et al*[39]). Seventh, ASL and DSC may show hyperintensities in macrovascular structures. Those macrovascular signals may have had an influence on our correlation analysis and may explain overestimation of CBF in hyperperfused areas (see Bland–Altman plots in Figure 3B). Finally, although a single-shot 3D GRASE ASL readout has numerous advantages, a limitation is the blurring in slice direction caused by T2 decay that might hamper a correlation analysis. Tan *et al*[40] used a combination of 3D GRASE and a PROPELLER trajectory (3DGP) that minimized through plane blurring without loss of sensitivity or increasing acquisition time. Another way of controlling blurring along 3D direction is by segmenting the readout echo train.

In conclusion, we showed that a 3D GRASE readout at multi-TIs allows for the correction of long ATTs in patients with chronic steno-occlusive disease within a clinically feasible acquisition time. Our results are promising for the transfer of ASL to the general practice. More efficient labeling schemes and susceptibility artifact correction should be investigated in upcoming studies.

DISCLOSURE/CONFLICT OF INTEREST

JS reports the following board memberships, consultancies and/or payments for lectures including service on speaker's bureaus: Boehringer-Ingelheim, Sanofi, Bayer, Pfizer and Maquet. MG declares that he is collaborating with Siemens on sequence development and received funding from Siemens in the past. Furthermore he is CEO of mediri GmbH in Heidelberg. The remaining authors declare no conflict of interest.

REFERENCES

1 Detre JA, Leigh JS, Williams DS, Koretsky AP. Perfusion imaging. *Magn Reson Med* 1992; **23**: 37–45.
2 Detre JA, Rao H, Wang DJ, Chen YF, Wang Z. Applications of arterial spin labeled MRI in the brain. *J Magn Reson Imaging* 2012; **35**: 1026–1037.
3 Wintermark M, Sesay M, Barbier E, Borbély K, Dillon WP, Eastwood JD *et al.* Comparative overview of brain perfusion imaging techniques. *Stroke* 2005; **36**: e83–e99.
4 Pizzini FB, Farace P, Manganotti P, Zoccatelli G, Bongiovanni LG, Golay X *et al.* Cerebral perfusion alterations in epileptic patients during peri-ictal and post-ictal phase: PASL vs DSC-MRI. *Magn Reson Imaging* 2013; **31**: 1001–1005.
5 White CM, Pope WB, Zaw T, Qiao J, Naeini KM, Lai A *et al.* Regional and voxel-wise comparisons of blood flow measurements between dynamic susceptibility contrast magnetic resonance imaging (DSC-MRI) and arterial spin labeling (ASL) in brain tumors. *JNeuroimaging* 2014; **24**: 23–30.
6 Mirasol RV, Bokkers RPH, Hernandez DA, Merino JG, Luby M, Warach S *et al.* Assessing reperfusion with whole-brain arterial spin labeling a noninvasive alternative to Gadolinium. *Stroke* 2014; **45**: 456–461.

7 Wang DJJ, Alger JR, Qiao JX, Gunther M, Pope WB, Saver JL *et al.* Multi-delay multi-parametric arterial spin-labeled perfusion MRI in acute ischemic stroke -- comparison with dynamic susceptibility contrast enhanced perfusion imaging. *NeuroImage* 2013; **3**: 1–7.
8 Hirai T, Kitajima M, Nakamura H, Okuda T, Sasao A, Shigematsu Y *et al.* Quantitative blood flow measurements in gliomas using arterial spin-labeling at 3T: Intermodality Agreement and Inter- and Intraobserver Reproducibility Study. *Am J Neuroradiol* 2011; **32**: 2073–2079.
9 Mutke MA, Madai VI, von Samson-Himmelstjerna FC, Zaro Weber O, Revankar GS, Martin SZ *et al.* Clinical evaluation of an arterial-spin-labeling product sequence in steno-occlusive disease of the brain. *PLoS One* 2014; **9**; e87143.
10 Günther M, Oshio K, Feinberg DA. Single-shot 3D imaging techniques improve arterial spin labeling perfusion measurements. *Magn Reson Med* 2005; **54**: 491–498.
11 Healthcare Siemenes Global Webside:2014 syngo ASL https://www.healthcare.siemens.com/magnetic-resonance-imaging/options-and-upgrades/clinical-applications/asl.htm.
12 Alsop DC, Detre JA, Golay X, Günther M, Hendrikse J, Hernandez-Garcia L *et al.* Recommended implementation of arterial spin-labeled perfusion MRI for clinical applications: a consensus of the ISMRM perfusion study group and the European consortium for ASL in dementia. *Magn Reson Med* e-pub ahead of print 8 April 2014doi:10.1002/mrm.25197.
13 Luh W-M, Wong EC, Bandettini PA, Hyde JS. QUIPSS II with thin-slice TI1 periodic saturation: a method for improving accuracy of quantitative perfusion imaging using pulsed arterial spin labeling. *Magn Reson Med* 1999; **41**: 1246–1254.
14 Wong EC, Buxton RB, Frank LR. Quantitative imaging of perfusion using a single subtraction (QUIPSS and QUIPSS II). *Magn Reson Med* 1998; **39**: 702–708.
15 Buxton RB, Frank LR, Wong EC, Siewert B, Warach S, Edelman RR. A general kinetic model for quantitative perfusion imaging with arterial spin labeling. *Magn Reson Med* 1998; **40**: 383–396.
16 Zaro-Weber O, Moeller-Hartmann W, Heiss W-D, Sobesky J. Influence of the arterial input function on absolute and relative perfusion-weighted imaging penumbral flow detection a validation with 15O-water positron emission tomography. *Stroke* 2012; **43**: 378–385.
17 Wu O, Østergaard L, Weisskoff RM, Benner T, Rosen BR, Sorensen AG. Tracer arrival timing-insensitive technique for estimating flow in MR perfusion-weighted imaging using singular value decomposition with a block-circulant deconvolution matrix. *Magn Reson Med* 2003; **50**: 164–174.
18 Matsushima S, Kubota T, Yamada K, Akazawa K, Masunami T, Ito H *et al.* Effect of vascular stenosis on perfusion-weighted imaging; differences between calculation algorithms. *J Magn Reson Imaging* 2008; **27**: 1103–1108.
19 MacIntosh BJ, Filippini N, Chappell MA, Woolrich MW, Mackay CE, Jezzard P. Assessment of arterial arrival times derived from multiple inversion time pulsed arterial spin labeling MRI. *Magn Reson Med* 2010; **63**: 641–647.
20 Warrens MJ. Inequalities between multi-rater kappas. *Adv Data Analysis Classification* 2010; **4**: 271–286.
21 Randolph JJ (2008) Online Kappa Calculator http://justusrandolph.net/kappa/.
22 Čížek J, Herholz K, Vollmar S, Schrader R, Klein J, Heiss W-D. Fast and robust registration of PET and MR images of human brain. *NeuroImage* 2004; **22**: 434–442.
23 Tatu L, Moulin T, Vuillier F, Bogousslavsky J. Arterial territories of the human brain. In: Paciaroni M, Agnelli G, Caso V, Bogousslavsky J (eds) *Frontiers of Neurology and Neuroscience* vol. 30. KARGER: Basel, 2012, pp 99–110.
24 Smith SM, Jenkinson M, Woolrich MW, Beckmann CF, Behrens TEJ, Johansen-Berg H *et al.* Advances in functional and structural MR image analysis and implementation as FSL. *NeuroImage* (2004); **23**(Supplement 1):S208–S219.
25 Andersson JLR, Skare S, Ashburner J. How to correct susceptibility distortions in spin-echo echo-planar images: application to diffusion tensor imaging. *NeuroImage* 2003; **20**: 870–888.
26 Hendrikse J, Petersen ET, Golay X. Vascular disorders: insights from arterial spin labeling. *Neuroimag Clin N Am* 2012; **22**: 259–269.
27 Golay X, Guenther M. Arterial spin labelling: final steps to make it a clinical reality. *Magn Reson Mater Phys Biol Med* 2012; **25**: 79–82.
28 MacIntosh BJ, Lindsay AC, Kylintireas I, Kuker W, Günther M, Robson MD *et al.* Multiple inflow pulsed arterial spin-labeling reveals delays in the arterial arrival time in minor stroke and transient ischemic attack. *Am J Neuroradiol* 2010; **31**: 1892–1894.
29 Yun TJ, Sohn C-H, Han MH, Kang H-S, Kim JE, Yoon B-W *et al.* Effect of delayed transit time on arterial spin labeling: correlation with dynamic susceptibility contrast perfusion magnetic resonance in Moyamoya disease. *Invest Radiol* 2013; **48**: 795–802.
30 Qiu D, Straka M, Zun Z, Bammer R, Moseley ME, Zaharchuk G. CBF measurements using multidelay pseudocontinuous and velocity-selective arterial spin labeling in patients with long arterial transit delays: comparison with xenon CT CBF. *J Magn Reson Imaging* 2012; **36**: 110–119.
31 Zaharchuk G, Straka M, Marks MP, Albers GW, Moseley ME, Bammer R. Combined arterial spin label and dynamic susceptibility contrast measurement of cerebral blood flow. *Magn Reson Med* 2010; **63**: 1548–1556.
32 Bokkers RP, Bremmer JP, van Berckel BN, Lammertsma AA, Hendrikse J, Pluim JP *et al.* Arterial spin labeling perfusion MRI at multiple delay times: a correlative study with H215O positron emission tomography in patients with symptomatic carotid artery occlusion. *J Cereb Blood Flow Metab* 2009; **30**: 222–229.
33 Kamano H, Yoshiura T, Hiwatashi A, Abe K, Togao O, Yamashita K *et al.* Arterial spin labeling in patients with chronic cerebral artery steno-occlusive disease: correlation with 15O-PET. *Acta Radiologica (Stockholm, Sweden: 1987)* 2012; **54**: 99–106.
34 Uchihashi Y, Hosoda K, Zimine I, Fujita A, Fujii M, Sugimura K *et al.* Clinical application of arterial spin-labeling MR imaging in patients with carotid stenosis: quantitative comparative study with single-photon emission CT. *Am J Neuroradiol* 2011; **32**: 1545–1551.
35 Wang R, Yu S, Alger JR, Zuo Z, Chen J, Wang R *et al.* Multi-delay arterial spin labeling perfusion MRI in moyamoya disease–comparison with CT perfusion imaging. *Eur Radiol* 2014; **24**: 1135–1144.
36 Ruthotto L, Kugel H, Olesch J, Fischer B, Modersitzki J, Burger M *et al.* Diffeomorphic susceptibility artifact correction of diffusion-weighted magnetic resonance images. *Phys Med Biol* 2012; **57**: 5715–5731.
37 Zaharchuk G. Arterial spin labeling for acute stroke: practical considerations. *Transl Stroke Res* 2012; **3**: 228–235.
38 Noguchi T, Kawashima M, Irie H, Ootsuka T, Nishihara M, Matsushima T *et al.* Arterial spin-labeling MR imaging in moyamoya disease compared with SPECT imaging. *Eur J Radiol* 2011; **80**: e557–e562.
39 Vidorreta M, Wang Z, Rodríguez I, Pastor MA, Detre JA, Fernández-Seara MA. Comparison of 2D and 3D single-shot ASL perfusion fMRI sequences. *NeuroImage* 2013; **66**: 662–671.
40 Tan H, Hoge WS, Hamilton CA, Gunther M, Kraft RA. 3D GRASE PROPELLER: improved image acquisition technique for arterial spin labeling perfusion imaging. *Magn Reson Med* 2011; **66**: 168–173.

Supplementary Information accompanies the paper on the Journal of Cerebral Blood Flow & Metabolism website (http://www.nature.com/jcbfm)